A Hybrid Phase-Flow Method for solving the Liouville Equation in Bounded Domain*

Hao Wu,[†] and Xu Yang[‡]

October 9, 2009

Abstract

The phase flow method was originally introduced in [28] which can efficiently compute the autonomous ordinary differential equations. In [13], it was generalized to solve the Hamiltonian system where the Hamiltonian contains discontinuous functions, for example discontinuous potential or wave speed. However, both these works require the flow map constructed on an *invariant* manifold. This could lead to an expensive computational cost when the invariant domain is big or even unbounded.

In this paper, following the idea of [13], we propose a hybrid phase-flow method for solving the Liouville equation in the bounded domain where the flow map sits in the *variant* manifold of the *traditional* phase flow map. Moreover, with the help of some proper boundary conditions, this hybrid phase flow method could help reduce the numerical difficulty when the *invariant* manifold of the phase flow given by the Liouville equation is big or unbounded. Analysis of the numerical stability and convergence is given for the Liouville equation with the inflow boundary condition. We also verify the accuracy and efficiency of this algorithm by several examples related to the semiclassical limit of the Schrödinger equation.

Key words: phase-flow method, Liouville equation, high frequency waves, particle method, Hamiltonian system

1   Introduction

In recent years the computation of the high frequency waves has received lots of attention due to its importance in seismology, electromagnetic waves and

---

†Department of Mathematical Sciences, Tsinghua University, Beijing, 10084, China (hwu@tsinghua.edu.cn)

‡Program in Applied and Computational Mathematics, Princeton University, NJ 08544, USA (xuyang@math.princeton.edu)

quantum mechanics. A series of efficient numerical methods for computing the high frequency waves has been developed with the helpful tools of WKB analysis [15, 1, 4], the level set framework [11, 9, 2] and Gaussian beam methods [19, 21, 24, 14] etc. Some nice reviews are given in [3, 22] and related references. In most of these methods, one needs to deal with the following Liouville equation

$$f_t + \nabla_{\boldsymbol{\xi}} H \cdot \nabla_{\boldsymbol{x}} f - \nabla_{\boldsymbol{x}} H \cdot \nabla_{\boldsymbol{\xi}} f = 0, \ t > 0, \ \boldsymbol{x}, \boldsymbol{\xi} \in \mathbb{R}^d, \tag{1}$$

which serves as the semiclassical limit of the linear high frequency waves ([3, 7, 18]). Here $f(t, \boldsymbol{x}, \boldsymbol{\xi}) \geq 0$ is the probability density function at time t, position $\boldsymbol{x}$ and velocity $\boldsymbol{\xi}$, and the Hamiltonian function $H = H(\boldsymbol{x}, \boldsymbol{\xi})$: $\mathbb{R}^{2d} \to \mathbb{R}$ is a function of $\boldsymbol{x}$ and $\boldsymbol{\xi}$ only. We consider equation (1) within the following bounded domain

$$M = \left\{ (\boldsymbol{x}, \boldsymbol{\xi}) \in \mathbb{R}^{2d} \mid \boldsymbol{x} \in X, \ H_{\min} \leq H(\boldsymbol{x}, \boldsymbol{\xi}) \leq H_{\max} \right\}, \tag{2}$$

where $X \subset \mathbb{R}^d$ is bounded and closed in the configuration space.

The particle method for the Liouville equation (1) is based on solving the following time-reversal Hamiltonian system (3)-(4),

$$\frac{\mathrm{d}\boldsymbol{x}}{\mathrm{d}t} = -\nabla_{\boldsymbol{\xi}} H, \tag{3}$$

$$\frac{\mathrm{d}\boldsymbol{\xi}}{\mathrm{d}t} = \nabla_{\boldsymbol{x}} H. \tag{4}$$

In [28], Ying and Candés proposed the novel phase flow method which computed (3)-(4) for multiple initial conditions efficiently and successfully. This method was later generalized to solve (3)-(4) in heterogeneous media in [13]. The key idea of the phase flow method is to construct the flow map $h_t : \mathbb{R}^{2d} \to \mathbb{R}^{2d}$ by making use of its group property and numerical interpolation efficiently on an *invariant* manifold M, where h_t is defined by $h_t(\boldsymbol{x}_0, \boldsymbol{\xi}_0) = (\boldsymbol{x}(t), \boldsymbol{\xi}(t))$ and the manifold M is invariant if $h_t(M) \subset M$.

However, the restriction of M being *invariant* may not hold here since the Liouville equation (1) is considered in a bounded domain which may not satisfy $h_t(M) \subset M$. On the other hand, even though we consider (1) in the whole space, the restriction of M being *invariant* could cause expensive computational cost when the size of M is large or even unbounded. One may encounter such cases in many common Hamiltonian systems. For example, if we consider the Hamiltonian in classic mechanics $H = \frac{1}{2}|\boldsymbol{\xi}|^2 + V(\boldsymbol{x})$ and the potential $V(\boldsymbol{x}) = 0$, the *invariant* domain for the phase flow of (3)-(4) is $\{(\boldsymbol{x}, \boldsymbol{\xi}) | \boldsymbol{x} \in \mathbb{R}^d, \ \boldsymbol{\xi} \in \Xi\}$ which is certainly unbounded.

Following the idea of [13], we develop a hybrid phase flow method in this paper to solve the Liouville equation (1) in a bounded domain where the new flow map sits on the *variant* manifold of the *traditional* phase flow map.

2

This also offers an option to reduce the numerical difficulty in the traditional phase flow method when the *invariant* manifold yielded by the Liouville equation is big or unbounded by using some proper boundary conditions.

We consider the following inflow boundary condition for (1),

$$f(\boldsymbol{x},\boldsymbol{\xi},t)|_{x\in\partial X,\boldsymbol{\xi}\cdot\boldsymbol{n}>0} = g(\boldsymbol{x},\boldsymbol{\xi},t), \tag{5}$$

where $\boldsymbol{n}$ denotes the normal direction of the boundary ∂X, and the initial condition is

$$f(\boldsymbol{x}_0,\boldsymbol{\xi}_0,0) = f_0(\boldsymbol{x}_0,\boldsymbol{\xi}_0). \tag{6}$$

We consider (3)-(4) with the initial conditions

$$\boldsymbol{x}(0) = \boldsymbol{x}_0, \ \boldsymbol{\xi}(0) = \boldsymbol{\xi}_0, \tag{7}$$

and define the phase flow solution $h_T(\boldsymbol{x}_0,\boldsymbol{\xi}_0)$ by the following rules (for $T > 0$):

1. $\boldsymbol{x}(t;\boldsymbol{x}_0,\boldsymbol{\xi}_0) \in \mathring{X}, \ \forall t \in [0,T]$. This means the particle stays inside the configuration space domain X, then the phase flow solution are given by

$$h_T(\boldsymbol{x}_0,\boldsymbol{\xi}_0) = (\boldsymbol{x}(T;\boldsymbol{x}_0,\boldsymbol{\xi}_0),\boldsymbol{\xi}(T;\boldsymbol{x}_0,\boldsymbol{\xi}_0)). \tag{8}$$

2. $\exists t \in [0,T], \ \boldsymbol{x}(t;\boldsymbol{x}_0,\boldsymbol{\xi}_0) \in \partial X$. In this case the particle trajectory would collide with the boundary ∂X, then the phase flow solution are given by

$$h_T(\boldsymbol{x}_0,\boldsymbol{\xi}_0) = (\boldsymbol{x}(t';\boldsymbol{x}_0,\boldsymbol{\xi}_0),\boldsymbol{\xi}(t';\boldsymbol{x}_0,\boldsymbol{\xi}_0)), \tag{9}$$

where the $t' = t'(\boldsymbol{x}_0,\boldsymbol{\xi}_0)$ is the first arrival time

$$t' = \inf\{t \in [0,T]\big|\boldsymbol{x}(t;\boldsymbol{x}_0,\boldsymbol{\xi}_0) \in \partial X\}. \tag{10}$$

Then the solution $f(T,\boldsymbol{x},\boldsymbol{\xi})$ of (1) is given by the method of characteristics,

$$f(\boldsymbol{x},\boldsymbol{\xi},T) = \begin{cases} f_0(h_T(\boldsymbol{x},\boldsymbol{\xi})), & \text{the particle moves inside } X, \\ g(h_T(\boldsymbol{x},\boldsymbol{\xi}),T - t'(\boldsymbol{x},\boldsymbol{\xi})), & \text{the particle coincides with boundary } \partial X. \end{cases} \tag{11}$$

Remark 1.1 *Sometimes, we are interested in reflection boundary condition*

$$f(\boldsymbol{x},\boldsymbol{\xi},t)|_{x\in\partial X,\boldsymbol{\xi}\cdot\boldsymbol{n}>0} = f(\boldsymbol{x},-\boldsymbol{\xi},t), \tag{12}$$

then $f(T,\boldsymbol{x},\boldsymbol{\xi})$ is recovered as

$$f(\boldsymbol{x},\boldsymbol{\xi},T) = f_0(h_T(\boldsymbol{x},\boldsymbol{\xi})). \tag{13}$$

Here h_T can be constructed using the traditional idea of hybrid phase-flow method[13], considering the boundary condition as the interface with full reflection.

We organize the paper as follows. In Section 2, we introduce the hybrid phase-flow method which solves the Liouville equation in a bounded domain. The analysis of the numerical stability and convergency is discussed in Section 3. Combined with the algorithm developed in [13], this hybrid phase flow method could have lots of applications in computing the high frequency waves which we will discuss in Section 4. In Section 5, we make some conclusive remarks.

2   The hybrid phase flow method

In this section we systematically introduce how to construct h_t on the bounded domain M at time $t = T$ efficiently. We select a small time step $\tau > 0$ and an integer constant $K \geq 1$ such that $B = (T/\tau)^{1/K}$ is an integer power of 2. The general procedure is described as follows:

1. Discretization. Start with a uniform or quasi-uniform grid M_h on M.

2. Initialization. Compute an approximation of h_τ.

   (a) For each $(\boldsymbol{x}_0, \boldsymbol{\xi}_0) \in M_h$, $h_\tau(\boldsymbol{x}_0, \boldsymbol{\xi}_0)$ is computed by numerical Hamiltonian solver Θ_τ on bounded domain, which is described in details in subsection 2.1.

   (b) The value of h_τ at any other point is given via either a local interpolation $\mathcal{I}$ (for regular particles) or numerical Hamiltonian solver Θ_τ (for special particles).

3. Loop. Construct $h_{B^{k+1}\tau}$ from $h_{B^k\tau}$, loop for $b = 1, \cdots, B - 1$:

   (a) For each $(\boldsymbol{x}_0, \boldsymbol{\xi}_0) \in M_h$

   $$h_{(b+1)\cdot B^k\tau}(\boldsymbol{x}_0, \boldsymbol{\xi}_0) = h_{B^k\tau}(h_{b\cdot B^k\tau}(\boldsymbol{x}_0, \boldsymbol{\xi}_0)) \tag{14}$$

   (b) For other points, use the local interpolation $\mathcal{I}$ (for regular particles) or the numerical Hamiltonian solver Θ_τ (for special particles).

The detailed implementation of this algorithm is given in Section 2.2.

2.1   A numerical Hamiltonian solver for bounded domain

In this subsection, following the idea of [10] we design the numerical Hamiltonian solver

$$
\begin{aligned}
\Theta_{\Delta t}: \quad M \subset \mathbb{R}^{2d} \quad &\to \quad M \subset \mathbb{R}^{2d} \\
(\boldsymbol{x}^n, \boldsymbol{\xi}^n) \quad &\to \quad (\boldsymbol{x}^{n+1}, \boldsymbol{\xi}^{n+1})
\end{aligned}
$$

for the Hamiltonian system (3)-(4) on the bounded domain M given by (2). For convenience, we denote $\Gamma_{\Delta t}(\boldsymbol{x}, \boldsymbol{\xi}) : \mathbb{R}^{2d} \to \mathbb{R}^{2d}$ as the one-step standard sympletic numerical solvers given in [6, 16], for example, the Verlet scheme.

1. Estimate the updated position and velocity of particle $(\boldsymbol{x}^*, \boldsymbol{\xi}^*) = \Gamma_{\Delta t}(\boldsymbol{x}^n, \boldsymbol{\xi}^n)$.

2. If $\boldsymbol{x}^* \in \mathring{X}$, i.e., the particle moves inside the bounded domain X during $[t^n, t^{n+1}]$, we set $(\boldsymbol{x}^{n+1}, \boldsymbol{\xi}^{n+1}) = (\boldsymbol{x}^*, \boldsymbol{\xi}^*)$.

3. Otherwise,

   (a) Approximate the first arrival time $\Delta t^\star = \frac{d(\boldsymbol{x}^n)}{d(\boldsymbol{x}^*) + d(\boldsymbol{x}^n)} \Delta t$, where $d(\boldsymbol{x})$ is the distance to the boundary ∂X.

   (b) Estimate the first arrival position and velocity $(\boldsymbol{x}^\star, \boldsymbol{\xi}^\star) = \Gamma_{\Delta t^\star}(\boldsymbol{x}, \boldsymbol{\xi})$.

   (c) Set $(\boldsymbol{x}^{n+1}, \boldsymbol{\xi}^{n+1}) = (\boldsymbol{x}^\star, \boldsymbol{\xi}^\star)$.

Remark 2.1 *As it will be proved in Section 3, the numerical Hamiltonian solver Θ_τ converges at second order. Its numerical accuracy can be improved by choosing higher order sympletic numerical solvers and approximating the first arrival time more accurate.*

2.2 The detailed implementation

We describe the hybrid phase flow method for the bounded domain in details here. The key issue of it is to identify different types of particles. First we introduce several symbols for convenience.

Symbol 1 $N_i^{(k)} = (\boldsymbol{x}_i^{(k)}, \boldsymbol{\xi}_i^{(k)}) \in M$ *is the position and velocity of the particle after k iterations, which initially starts at $N_i^{(0)} = (\boldsymbol{x}_i^{(0)}, \boldsymbol{\xi}_i^{(0)})$. Note that the initial mesh $M_h = \{N_i^{(0)}, \forall i\}$.*

Symbol 2 *Denote G_j as the mesh cells, and $\mathcal{N}(G_j) = \{N_{j_1}^{(0)}, \cdots, N_{j_l}^{(0)}\}$ be the set of all the vertices (mesh points) of G_j. Define $\mathcal{G}(\boldsymbol{x}, \boldsymbol{\xi}) = j$, if $(\boldsymbol{x}, \boldsymbol{\xi}) \in G_j$.*

Symbol 3 *Denote $\mathcal{S}(N_i^{(0)})$ as the current status of the particle initially starting at $N_i^{(0)}$,*

$$\mathcal{S}(N_i^{(0)}) = \begin{cases} 0, & \text{if particle has coincided with the boundary } \partial X, \\ 1, & \text{otherwise.} \end{cases}$$

Symbol 4 *Define $\mathcal{I}_1$ as the evolutional interpolation function, and*

$$(\boldsymbol{y}^*, \boldsymbol{\eta}^*) = \mathcal{I}_1\left((\boldsymbol{x}^1, \boldsymbol{\xi}^1), \cdots, (\boldsymbol{x}^l, \boldsymbol{\xi}^l), (\boldsymbol{y}^1, \boldsymbol{\eta}^1), \cdots, (\boldsymbol{y}^l, \boldsymbol{\eta}^l); (\boldsymbol{x}^*, \boldsymbol{\xi}^*)\right), \quad (15)$$

where $\mathcal{I}_1$ interpolates at points $(\boldsymbol{x}^i, \boldsymbol{\xi}^i) \in M$, the values $(\boldsymbol{y}^i, \boldsymbol{\eta}^i) \in M(i = 1, \cdots, l)$. For $(\boldsymbol{x}^*, \boldsymbol{\xi}^*) \in M$, $\mathcal{I}_1$ gives its value $(\boldsymbol{y}^*, \boldsymbol{\eta}^*) \in M$.

Symbol 5 *Define $\mathcal{I}_2$ as the first arrival interpolation function, and*

$$(t^*, \boldsymbol{y}^*, \boldsymbol{\eta}^*) = \mathcal{I}_2\left((\boldsymbol{x}^1, \boldsymbol{\xi}^1), \cdots, (\boldsymbol{x}^l, \boldsymbol{\xi}^l), (t^1, \boldsymbol{y}^1, \boldsymbol{\eta}^1), \cdots, (t^l, \boldsymbol{y}^l, \boldsymbol{\eta}^l); (\boldsymbol{x}^*, \boldsymbol{\xi}^*)\right),$$
(16)

where $\mathcal{I}_2$ interpolates through points $(\boldsymbol{x}^i, \boldsymbol{\xi}^i) \in M$, the values t^i, $\boldsymbol{y}^i$ and $\boldsymbol{\eta}^i$ denote the first arrival time, position and velocity, respectively, in which $(\boldsymbol{y}^i, \boldsymbol{\eta}^i) \in M$ and $\boldsymbol{y}^i \in \partial X$. For $(\boldsymbol{x}^*, \boldsymbol{\xi}^*) \in M$, $\mathcal{I}_2$ gives its value $(t^*, \boldsymbol{y}^*, \boldsymbol{\eta}^*)$ with $(\boldsymbol{y}^*, \boldsymbol{\eta}^*) \in M$ and $\boldsymbol{y}^* \in \partial X$.

Symbol 6 *Let $t' = t'(\boldsymbol{x}, \boldsymbol{\xi}) : M \to [0, +\infty) \cup \{-1\}$ be the first arrival time when the particle initially at $(\boldsymbol{x}, \boldsymbol{\xi})$ collides with the boundary ∂X. If the particle never collides with the boundary ∂X, it will be set to be -1.*

Now we give the detailed implementation of the algorithm:

1. Discretization. Assume we start with a uniform or quasi-uniform mesh $M_h = \{N_i^{(0)} | i = 1, \cdots, I\}$, then G_j and $\mathcal{N}(G_j)$ $(j = 1, \cdots, J)$ are well defined. The stopping time is $t = T$. The small time τ and number of iterations $K \geq 1$ is selected to be satisfied $B = (T/\tau)^{1/K}$ is an integer power of 2.

2. Initialization. Set $k = 1$. For $i = 1, \cdots, I$

$$N_i^{(1)} = \Theta_\tau(N_i^{(0)}).$$
(17)

Since the numerical Hamiltonian solver Θ_τ can automatically check whether the particle trajectory collides with the boundary during $[0, \tau]$, we can set

$$\mathcal{S}(N_i^{(0)}) = 0, \ t'(N_i^{(0)}) = \Delta t^\star,$$
(18)

for the particles that collide with the boundary, or

$$\mathcal{S}(N_i^{(0)}) = 1, \ t'(N_i^{(0)}) = -1,$$
(19)

for the particles that stay inside the domain X.

3. Loop at the kth iteration. For $i = 1, \cdots, I$

$$N_i^{(k+1)} = N_i^{(k)}.$$
(20)

Loop the below part for $b = 1, \cdots, B - 1$.

- For those particles satisfying $\mathcal{S}(N_i^{(0)}) = 1$, there is $j = \mathcal{G}(N_i^{(k+1)})$ such that $N_i^{(k+1)} \in G_j$. We check the status value of all the vertices $N_m^{(0)} \in \mathcal{N}(G_j)$, $m \in \{j_1, j_2, \cdots, j_l\}$ to update $N_i^{(k+1)}$.

(a) If $\mathcal{S}(N_m^{(0)}) = 0$, $\forall m \in \{j_1, j_2, \cdots, j_l\}$, $N_i^{(k+1)}$ is called the boundary colliding particle, and we compute the first arrival time $t'(N_i^{(0)})$ and the value of $N_i^{(k+1)}$ by local interpolation:

$$
\left(t'(N_i^{(0)}), N_i^{(k+1)}\right) = \mathcal{I}_2\left(N_{j1}^{(0)}, \cdots, N_{jl}^{(0)}, \left(t'(N_{j1}^{(0)}), N_{j1}^{(k)}\right), \right.
$$
$$
\left. \cdots, \left(t'(N_{jl}^{(0)}), N_{jl}^{(k)}\right); N_i^{(k+1)}\right). \quad (21)
$$

The particle status value is updated as

$$
\mathcal{S}(N_i^{(0)}) = 0. \quad (22)
$$

(b) If $\mathcal{S}(N_m^{(0)}) = 1$, $\forall m \in \{j_1, j_2, \cdots, j_l\}$, $N_i^{(k+1)}$ is called the standard evolutional particle, and we define the new value of $N_i^{(k+1)}$ by the local interpolation:

$$
N_i^{(k+1)} = \mathcal{I}_1\left(N_{j1}^{(0)}, \cdots, N_{jl}^{(0)}, N_{j1}^{(k)}, \cdots, N_{jl}^{(k)}; N_i^{(k+1)}\right). \quad (23)
$$

The last two types of particles are named *regular* particles.

(c) Otherwise if $\mathcal{S}(N_m^{(0)}) = 0$ for only some $m \in \{j_1, j_2, \cdots, j_l\}$, $N_i^{(k+1)}$ is called the *special* particle, and we decide the new value of $N_i^{(k+1)}$ by the numerical Hamiltonian solver Θ_τ: update the value of $N_i^{(k+1)}$ for B^k times by

$$
N_i^{(k+1)} = \Theta_\tau(N_i^{(k+1)}). \quad (24)
$$

If the particle collides with the boundary at some step k', the first arrival time is

$$
t'(N_i^{(0)}) = (b \cdot B^k + k' - 1)\tau + \Delta t^\star. \quad (25)
$$

The particle status value is updated as

$$
\mathcal{S}(N_i^{(0)}) = 0. \quad (26)
$$

- For particle satisfies $\mathcal{S}(N_i^{(0)}) = 0$, which means the particle has already collided with the boundary, its value doesn't change since then.

4. If $k + 1 = K$, stop. Otherwise we let $k = k + 1$ and go to step 3.

By the above procedure, we obtain the position and velocity $N_i^{(K)}$ of the particle at time $T = B^K \tau$, which initially starts at $N_i^{(0)} (i = 1, \cdots, I)$. For these particles colliding with the boundary, we also have an approximation of the first arrival time $t'(N_i^{(0)})$.

Remark 2.2 *Combined with the idea of [13], this algorithm could be easily generalized to the interface problem where the Hamiltonian contains discontinuous functions. We also study this case in the numerical examples later.*

Remark 2.3 *As discussed in [13], the number of special particles is estimated as $O(N^{2d-1})$ on a 2d-dimensional phase space lattice M_h with N particles in each direction. We also numerically verify this in Section 4. So the total computational complexity for the Hybrid phase-flow method is $O(N^{2d-1}L + N^{2d}L^{1/s})$ with $L = B^K$.*

3 Stability and convergence

In this section we analyze the stability and convergence for this hybrid phase flow method. For the sake of simplicity and clarity, we investigate the 1D problem in classical mechanics where the Hamiltonian $H : \mathbb{R}^2 \to \mathbb{R}$ is given by

$$H(x, \xi) = \frac{1}{2}\xi^2 + V(x),$$

in which the potential $V(x) \in C^\infty(X)$. The bounded and closed domain $X \subset \mathbb{R}$ is taken as $X = [-1, 1]$ without loss of generality. Then the right hand side of the Hamiltonian system (3)-(4)

$$F(x, \xi) = (-\xi, V'(x))^T$$

is smooth and has Lipschitz constant L on X.

3.1 Analysis of the algorithm stability

We first study the stability of the phase flow solution h_t under some reasonable assumptions that all the particles lie in the domain

$$D = \left\{ (x, \xi) \in \mathbb{R}^2 \,\middle|\, \big|H(x, \xi) - V(\pm 1)\big| > \epsilon_0 \right\}$$

where $\epsilon_0 > 0$ is a small parameter. This removes the physical unstable cases where the particles have zero velocity at the boundaries $x = \pm 1$ but will travel inside the domain M under small perturbations.

Theorem 3.1 *The phase flow solution h_t defined in Section 1 is stable on $D \cap M$, with the estimate*

$$\|h_t(x_1, \xi_1) - h_t(x_2, \xi_2)\| \le L_1 e^{L_2 t} \|(x_1, \xi_1) - (x_2, \xi_2)\|,$$

where L_1 and L_2 are constants.

Proof:(I) If $x(t'; x_i, \xi_i) \in \mathring{X}$, $\forall t' \in [0, t], i = 1, 2$, which means both the particles always stay inside X, it is easy to have

$$\|h_t(x_1, \xi_1) - h_t(x_2, \xi_2)\| \le e^{Lt} \|(x_1, \xi_1) - (x_2, \xi_2)\|, \tag{27}$$

by using Gronwall's inequality.

(II) If $\exists t' \in [0, t]$, $x(t'; x_i, \xi_i) \in \partial X$, $i = 1, 2$, which means at least one particle trajectory collides with the boundary ∂X. We can assume that there exists $t_a \in [0, t)$ satisfies:

   i. $x(t_a; x_1, \xi_1) \in \partial X$,

   ii. $x(t'; x_1, \xi_1) \in \mathring{X}$, $\forall t' \in [0, t_a)$,

   iii. $x(t'; x_2, \xi_2) \in \mathring{X}$, $\forall t' \in [0, t_a]$,

without loss of of generality. By (I) and the closeness of X, we have

$$\|h_{t_a}(x_1, \xi_1) - h_{t_a}(x_2, \xi_2)\| \le e^{L t_a} \|(x_1, \xi_1) - (x_2, \xi_2)\|. \tag{28}$$

Let

$$
\begin{aligned}
t_b &= t - t_a, \\
(x_3, \xi_3) &= h_{t_a}(x_1, \xi_1), \\
(x_4, \xi_4) &= h_{t_a}(x_2, \xi_2),
\end{aligned}
$$

then we have

$$
\begin{aligned}
\|h_t(x_1, \xi_1) - h_t(x_2, \xi_2)\| &= \|h_{t_b}(h_{t_a}(x_1, \xi_1)) - h_{t_b}(h_{t_a}(x_2, \xi_2))\| \\
&= \|h_{t_b}(x_3, \xi_3) - h_{t_b}(x_4, \xi_4)\| \\
&= \|(x_3, \xi_3) - h_{t_b}(x_4, \xi_4)\|. \tag{29}
\end{aligned}
$$

The last equality is due to $x_3 \in \partial X$. Without loss of generality we assume $x_3 = 1$, then the velocity $\xi_3 > \sqrt{2\epsilon_0}$ since $(x_3, \xi_3) \in D$. We will prove the conclusion by discussing the following two cases.

Case 1. $x(t'; x_4, \xi_4) \in \mathring{X}$, $\forall t' \in [0, t_b]$. We define a new phase flow solution

$$\widehat{h}_t(x_0, \xi_0) = (\widehat{x}(t; x_0, \xi_0), \widehat{\xi}(t; x_0, \xi_0)),$$

by extending the potential V in (3)-(4) to the semi-unbounded domain

$$
\widehat{V}(x) = \begin{cases}
V(1) + \frac{1}{2} V'(1)\zeta, & x \in [1 + \zeta, \infty), \\
-\frac{1}{2\zeta} V'(1)(x - 1)^2 + V'(1)(x - 1) + V(1), & x \in (1, 1 + \zeta), \\
V(x), & x \in [-1, 1],
\end{cases}
$$

9

where $\zeta = \min(\frac{1}{2}\epsilon_0, \frac{\epsilon_0}{|V'(1)|})$. It is easy to verify that $\widehat{V} \in C^1([-1, \infty))$ and $\widehat{F}$ also has Lipschitz constant $L' = \max(L, \frac{|V'(1)|}{\zeta})$ on $[-1, \infty)$. Then we have

$$\left\| \widehat{h}_t(x_3, \xi_3) - \widehat{h}_t(x_4, \xi_4) \right\| \leq e^{L't_b} \left\| (x_3, \xi_3) - (x_4, \xi_4) \right\|. \tag{30}$$

Since $\xi_3 > \sqrt{2\epsilon_0}$ and $\left| \frac{1}{2}V'(1)\zeta \right| < \frac{1}{2}\epsilon_0$, the velocity $\widehat{\xi}(t'; x_3, \xi_3) > 0$, $\forall t' \in [0, t_b]$, this induces $\widehat{x}(t_b; x_3, \xi_3) > x_3 > \widehat{x}(t_b; x_4, \xi_4) = x(t_b; x_4, \xi_4)$ and

$$
\begin{array}{rcl}
|x_3 - x(t_b; x_4, \xi_4)| & < & |\widehat{x}(t_b; x_3, \xi_3) - \widehat{x}(t_b; x_4, \xi_4)|, \\
|x_3 - \widehat{x}(t_b; x_3, \xi_3)| & < & |\widehat{x}(t_b; x_3, \xi_3) - \widehat{x}(t_b; x_4, \xi_4)|.
\end{array}
\tag{31}
$$

On the other hand, we have

$$
\begin{array}{rcl}
|\xi_3 - \xi(t_b; x_4, \xi_4)| & \leq & \left| \widehat{\xi}(t_b; x_3, \xi_3) - \widehat{\xi}(t_b; x_4, \xi_4) \right| + \left| \xi_3 - \widehat{\xi}(t_b; x_3, \xi_3) \right| \\
& \leq & \left| \widehat{\xi}(t_b; x_3, \xi_3) - \widehat{\xi}(t_b; x_4, \xi_4) \right| + L'' |x_3 - \widehat{x}(t_b; x_3, \xi_3)| \quad (32) \\
& < & \left| \widehat{\xi}(t_b; x_3, \xi_3) - \widehat{\xi}(t_b; x_4, \xi_4) \right| + L'' |\widehat{x}(t_b; x_3, \xi_3) - \widehat{x}(t_b; x_4, \xi_4)|.
\end{array}
$$
$$\tag{33}$$

The inequality (32) holds based on the observation that

$$\xi(x) = \sqrt{\xi_3^2 + 2(V(x_3) - \widehat{V}(x))}$$

has the Lipschitz constant $L'' = \max(L, \frac{|\widehat{V}'(x)|}{2\epsilon_0})$ on $[-1, +\infty)$.

Taking (28)-(31) and (33) we have

$$
\begin{array}{rcl}
\|h_t(x_1, \xi_1) - h_t(x_2, \xi_2)\| & = & \|(x_3, \xi_3) - h_{t_b}(x_4, \xi_4)\| \\
& \leq & (L'' + 1) \left\| \widehat{h}_t(x_3, \xi_3) - \widehat{h}_t(x_4, \xi_4) \right\| \\
& \leq & L_1 e^{L_2 t_b} \|(x_3, \xi_3) - (x_4, \xi_4)\| \\
& \leq & L_1 e^{L_2 t} \|(x_1, \xi_1) - (x_2, \xi_2)\|.
\end{array}
\tag{34}
$$

where $L_1 = L'' + 1$ and $L_2 = L'$ are constants.

Case 2. $\exists t' \in [0, t_b]$, $x(t'; x_4, \xi_4) \in \partial X$. Let $t_c \leq t_b$ be the first arrival time, it is easy to derive

$$
\begin{array}{rcl}
\|h_T(x_1, \xi_1) - h_T(x_2, \xi_2)\| & = & \|(x_3, \xi_3) - h_{t_b}(x_4, \xi_4)\| \\
& = & \|(x_3, \xi_3) - h_{t_c}(x_4, \xi_4)\| \\
& \leq & L_1 e^{L_2 t_c} \|(x_3, \xi_3) - (x_4, \xi_4)\| \\
& \leq & L_1 e^{L_2 t} \|(x_1, \xi_1) - (x_2, \xi_2)\|.
\end{array}
\tag{35}
$$

Summarizing all the cases (27), (34) and (35), we prove the theorem. $\blacksquare$

10

3.2 Convergence Analysis of the Algorithm

In this subsection we prove the convergence of the hybrid phase flow method.

Theorem 3.2 *The numerical Hamiltonian solver Θ_τ described in Section 2.1 converges with a second order accuracy on $D \cap M$.*

Proof: Since the one-step standard symplectic numerical solver Γ_Δ converges at second order when the particle stays inside the configuration space domain X, we only need to consider the situation when the particle is very near the boundary, i.e. for small enough Δt

$$\|\Theta_{\Delta t}(x_0, \xi_0) - h_{\Delta t}(x_0, \xi_0)\| \leq C_a \Delta t^2, \tag{36}$$

where the particle trajectory collides with the boundary ∂X in this short time Δt, and C_a is a positive constant.

Let Δt^* and $\Delta t^\star$ be the exact arrival time and the estimated arrival time respectively, and $(x_1, \xi_1) = h_{\Delta t^*}(x_0, \xi_0)$ be the position and velocity when the particle collide with the boundary ∂X. And we rewrite sympletic numerical solver $\Gamma_{\Delta t}$ as

$$\Gamma_{\Delta t}(x, \xi) = (x_\Gamma(\Delta t; x, \xi), \xi_\Gamma(\Delta t; x, \xi)).$$

Since $V(x) \in C^\infty(X)$, one could write the sympletic numerical solver as

$$\begin{aligned}
x_\Gamma(\Delta t; x, \xi) &= x + v_{11}(x, \xi)\Delta t + v_{21}(x, \xi)\Delta t^2 + O(\Delta t^3), \\
\xi_\Gamma(\Delta t; x, \xi) &= \xi + v_{12}(x, \xi)\Delta t + v_{22}(x, \xi)\Delta t^2 + O(\Delta t^3),
\end{aligned}$$

where

$$\|(v_{i1}, v_{i2})\| \leq C_i, \quad i = 1, 2.$$

By the approximation formula

$$\begin{aligned}
\Delta t^\star &= \frac{x_1 - x_0}{x_\Gamma(\Delta t; x_0, \xi_0) - x_0} \Delta t \\
&= \frac{x_1 - x_0}{v_{11} + v_{21}\Delta t} + O(\Delta t^2),
\end{aligned}$$

thus

$$\begin{aligned}
x_\Gamma(\Delta t^\star; x_0, \xi_0) - x_1 &= x_0 + v_{11}\Delta t^\star + v_{21}\Delta t^{\star 2} - x_1 + O(\Delta t^{\star 3}) \\
&= \frac{v_{21}\Delta t(x_0 - x_1)}{v_{11} + v_{21}\Delta t} + v_{21}\Delta t^{\star 2} + O(\Delta t^{\star 3}).
\end{aligned}$$

Furthermore

$$\begin{aligned}
|x_0 - x_1| &\leq |x_0 - x_\Gamma(\Delta t; x_0, \xi_0)| \\
&\leq |v_{11}|\Delta t + |v_{21}|\Delta t^2,
\end{aligned}$$

11

this implies that

$$|x_\Gamma(\Delta t^\star; x_0, \xi_0) - x_1| \leq D_1 \Delta t^2,$$

for $\Delta t > 0$ small enough.

Since the numerical solver Γ_Δ is sympletic preserving, we have

$$V(x_\Gamma(\Delta t^\star; x_0, \xi_0)) + \frac{1}{2}\xi_\Gamma^2(\Delta t^\star; x_0, \xi_0) = V(x_1) + \frac{1}{2}\xi_1^2,$$

which gives

$$
\begin{aligned}
|\xi_\Gamma(\Delta t^\star; x_0, \xi_0) - \xi_1| &\leq \frac{2\,|V(x_\Gamma(\Delta t^\star; x_0, \xi_0)) - V(x_1)|}{|\xi_\Gamma(\Delta t^\star; x_0, \xi_0) + \xi_1|} \\
&\leq \frac{2D_2\,|x_\Gamma(\Delta t^\star; x_0, \xi_0) - x_1|}{2\sqrt{\epsilon_0}} \\
&\leq \frac{D_1 D_2}{\sqrt{\epsilon_0}} \Delta t^2 = D_3 \Delta t^2.
\end{aligned}
$$

The inequality is based on that $V(x)$ is Lipschitz continuous on X and $(x_0, \xi_0) \in D \cap M$. Taking

$$C_a = D_1 + D_3,$$

proves (36).

For any fixed time T, we choose the time step Δt and the iteration time N such that $N\Delta t = T$. If the particle initially at (x_0, ξ_0) does not collide with the boundary ∂X, then

$$\|\Theta_{N\Delta t}(x_0, \xi_0) - h_T(x_0, \xi_0)\| = \|\Gamma_{N\Delta t}(x_0, \xi_0) - h_T(x_0, \xi_0)\| \leq C_b \Delta t^2,$$

where C_b is a constant independent of T. For the particle initially at (x_0, ξ_0) collides with the boundary ∂X, we denote T_1 as the boundary colliding time. We choose $t_1 \geq 0$ and an integer N_1 such that

$$T_1 = N_1 \Delta t + t_1, \text{ and } 0 \leq t_1 < \Delta t.$$

Then we have

$$
\begin{aligned}
\|\Theta_{N\Delta t}(x_0, \xi_0) - h_T(x_0, \xi_0)\| &= \|\Theta_{t'}(\Gamma_{N_1\Delta t}(x_0, \xi_0)) - h_{t'}(h_{N_1\Delta t}(x_0, \xi_0))\| \\
&\leq \|\Theta_{t'}(h_{N_1\Delta t}(x_0, \xi_0)) - h_{t'}(h_{N_1\Delta t}(x_0, \xi_0))\| + \\
&\quad \|\Theta_{t'}(\Gamma_{N_1\Delta t}(x_0, \xi_0)) - \Theta_{t'}(h_{N_1\Delta t}(x_0, \xi_0))\| \\
&\leq C_a \Delta t^2 + L_1 e^{L_2 t'} \|\Gamma_{N_1\Delta t}(x_0, \xi_0) - h_{N_1\Delta t}(x_0, \xi_0))\| \\
&\leq C_a \Delta t^2 + L_1 e^{L_2 t'} C_b \Delta t^2
\end{aligned}
$$

Taking

$$C_0 = \max\left(C_b, C_a + L_1 e^{L_2 t'} C_b\right),$$

we prove the theorem.∎

The idea of the proofs for the next lemma and theorem mostly follows those in [28] except with more careful discussions on the cases of boundary colliding particles and special particles.

Lemma 3.3 *For any multi-index γ with $|\gamma| = s \geq 2$, one has*

$$|\partial^\gamma h_t(x_0, \xi_0)| \leq C_s^1 e^{(2s-1)LT} \cdot t, \quad \forall (x_0, \xi_0) \in M_a,$$
$$|\partial^\gamma h_t(x_0, \xi_0)| \leq C_s^2, \quad \forall (x_0, \xi_0) \in M_b.$$

where C_s^ℓ, $\ell = 1, 2$ are constants and the sets $M_a = M_a(t)$ and $M_b = M_b(t)$ are defined by

$$\begin{aligned}
M_a &= \left\{ (x_0, \xi_0) \in D \cap M \big| x(t'; x_0, \xi_0) \in \mathring{X}, \forall t' \in [0, t] \right\}, \\
M_b &= \left\{ (x_0, \xi_0) \in D \cap M \big| \exists t' \in (0, t), \ s.t. \ x(t'; x_0, \xi_0) \in \partial X \right\}.
\end{aligned}$$

Proof: Lemma 2.3 in [28] gives

$$|\partial^\gamma h_t(x_0, \xi_0)| \leq C_s^1 e^{(2s-1)LT} t, \quad \forall (x_0, \xi_0) \in M_a.$$

For $(x_0, \xi_0) \in M_b$, one could easily see that there exists $l > 0$, for any $(x_0', \xi_0') \in D \cap M$ which satisfies

$$\left\| (x_0', \xi_0') - (x_0, \xi_0) \right\| < l,$$

$(x_0', \xi_0') \in M_b$ holds.

Moreover, if we choose $l < \frac{2}{L_1} e^{-L_2 T}$, then by the stability estimate

$$\left\| h_t(x_0', \xi_0') - h_t(x_0, \xi_0) \right\| < 2,$$

this implies $x(t; x_0, \xi_0) = x(t; x_0', \xi_0')$ because the boundaries are either $x = 1$ or $x = -1$. Therefore

$$\partial^\gamma x(t; x_0, \xi_0) = 0, \quad \forall (x_0, \xi_0) \in M_b.$$

By taking the derivatives of the energy conservation equation

$$\frac{1}{2} \xi^2(t; x_0, \xi_0) + V(x(t; x_0, \xi_0)) = \frac{1}{2} \xi_0^2 + V(x_0)$$

one has

$$\frac{1}{2} \partial^\gamma \left(\xi^2(t; x_0, \xi_0) \right) = \begin{cases} 1, & s = 2, \gamma = (0, 2) \\ V^{(s)}(x_0), & \gamma = (s, 0) \\ 0, & \text{otherwise.} \end{cases}$$

Here we will only prove the case of $s = 2$, while the other situations can be proved similarly by direct calculations.

For $\gamma = (0,2), (1,1)$ and $(2,0)$, we have

$$
\begin{aligned}
\xi_{\xi_0 \xi_0} &= \frac{1}{\xi} - \frac{\xi_0 \xi_{\xi_0}}{\xi^2} = \frac{\xi^2 - \xi_0^2}{\xi^3} = \frac{2(V(x_0) - V(x))}{\xi^3}, \\
\xi_{\xi_0 x_0} &= -\frac{\xi_0 \xi_{x_0}}{\xi^2} = -\frac{\xi_0 V'(x_0)}{\xi^3}, \\
\xi_{x_0 x_0} &= \frac{V''(x_0)}{\xi} - \frac{V'(x_0)\xi_{x_0}}{\xi^2} = \frac{\xi^2 V''(x_0) - V'^2(x_0)}{\xi^3}.
\end{aligned}
$$

Since $V(x) \in C^\infty(X)$, then we have $E_{(k)} \le \left| V^{(k)}(x) \right| \le E^{(k)}$ where $E_{(k)}$ and $E^{(k)}$ are constants. Hence

$$
\begin{aligned}
|\xi_{\xi_0 \xi_0}| &\le \frac{4E^{(0)}}{(2\epsilon_0)^{3/2}} = C_{(0,2)}, \\
|\xi_{\xi_0 x_0}| &\le \frac{\sqrt{2(H_{\max} - E_{(0)})E^{(1)}}}{(2\epsilon_0)^{3/2}} = C_{(1,1)}, \\
|\xi_{\xi_0 x_0}| &\le \frac{2(H_{\max} - E_{(0)})E^{(2)} + (E^{(1)})^2}{(2\epsilon_0)^{3/2}} = C_{(2,0)}.
\end{aligned}
$$

Letting $C_2^2 = C_{(0,2)} + C_{(1,1)} + C_{(2,0)}$ yields

$$
|\partial^\gamma h_t(x_0, \xi_0)| \le C_2^2, \quad \forall (x_0, \xi_0) \in M_b,
$$

which proves the theorem. ∎

Theorem 3.4 *Assume the accurate orders of the local interpolation schemes $\mathcal{I}_1$ and $\mathcal{I}_2$ are $\alpha \ge 1$ for functions sufficiently smooth, and the L^∞ norm of the linear interpolation on continuous functions is h-independent. We define the numerical error at time t as*

$$
\epsilon_t = \max_{(x,\xi) \in D \cap M} \left\| h_t(x, \xi) - \widetilde{h}_t(x, \xi) \right\|,
$$

where h_t is the exact solution and $\widetilde{h}_t$ is the numerical solution given in Section 2. Then it satisfies

$$
\epsilon_T \le C(\Delta t^2 + h),
$$

where $C > 0$ is constant.

Proof: We write $y = (x, \xi)$ as a short notation for particles. For the grid point y, one has

$$
\left\| h_{\Delta t}(y) - \widetilde{h}_{\Delta t}(y) \right\| \le C_0 \Delta t^2.
$$

14

If y is not on grids, we define $\mathcal{I}_j$ (resp. $\widetilde{\mathcal{I}}_j$) $j = 1, 2$ as the interpolation operators constructed from $h_{\Delta t}$ (resp. $\widetilde{h}_{\Delta t}$) for the boundary colliding and standard evolutional particles, then $\widetilde{h}_{\Delta t}(y) = \widetilde{\mathcal{I}}_j(y)$ and

$$\left\| h_{\Delta t}(y) - \widetilde{h}_{\Delta t}(y) \right\| \leq \begin{cases} \left\| \mathcal{I}_1(y) - \widetilde{\mathcal{I}}_1(y) \right\| + \| \mathcal{I}_1(y) - h_{\Delta t}(y) \|, & \text{for boundary colliding particles,} \\ \left\| \mathcal{I}_2(y) - \widetilde{\mathcal{I}}_2(y) \right\| + \| \mathcal{I}_2(y) - h_{\Delta t}(y) \|, & \text{for standard evolutional particles,} \\ \| \Theta_{\Delta t}(y) - h_{\Delta t}(y) \|, & \text{for special partiles.} \end{cases}$$

Denote N_1 and N_2 to be the h-independent norms of the interpolation operators $\mathcal{I}_1$ and $\mathcal{I}_2$, then

$$\left\| \mathcal{I}_1(y) - \widetilde{\mathcal{I}}_1(y) \right\| \leq N_1 \max_{y \in \{\text{grid points}\}} \left\| h_{\Delta t}(y) - \widetilde{h}_{\Delta t}(y) \right\| \leq C_0 N_1 \Delta t^2,$$

$$\left\| \mathcal{I}_2(y) - \widetilde{\mathcal{I}}_2(y) \right\| \leq N_2 \max_{y \in \{\text{grid points}\}} \left\| h_{\Delta t}(y) - \widetilde{h}_{\Delta t}(y) \right\| \leq C_0 N_2 \Delta t^2.$$

Since $\mathcal{I}_1$ and $\mathcal{I}_2$ are smooth interpolations, they have Lipschitz constants $L_{\mathcal{I}_1}$ and $L_{\mathcal{I}_2}$. As y is not a grid point, we can find a grid point y_1 such that

$$\| y - y_1 \| \leq h,$$

then

$$\begin{aligned} \| \mathcal{I}_1(y) - h_{\Delta t}(y) \| &\leq \| \mathcal{I}_1(y) - \mathcal{I}_1(y_1) \| + \| \mathcal{I}_1(y_1) - h_{\Delta t}(y_1) \| + \| h_{\Delta t}(y_1) - h_{\Delta t}(y) \| \\ &\leq L_{\mathcal{I}_1} \| y - y_1 \| + C_1 h^\alpha \max_{|\gamma| = \alpha} \sup_{y_0 \in M_b} \| \partial^\gamma h_{\Delta t}(y_0) \| + L_1 e^{L_2 \Delta t} \| y - y_1 \| \\ &\leq C_2 h + C_3 h^\alpha, \end{aligned}$$

and

$$\begin{aligned} \| \mathcal{I}_2(y) - h_{\Delta t}(y) \| &\leq \| \mathcal{I}_2(y) - \mathcal{I}_2(y_1) \| + \| \mathcal{I}_2(y_1) - h_{\Delta t}(y_1) \| + \| h_{\Delta t}(y_1) - h_{\Delta t}(y) \| \\ &\leq L_{\mathcal{I}_2} \| y - y_1 \| + C_4 h^\alpha \max_{|\gamma| = \alpha} \sup_{y_0 \in M_b} \| \partial^\gamma h_{\Delta t}(y_0) \| + L_1 e^{L_2 \Delta t} \| y - y_1 \| \\ &\leq C_5 h + C_6 h^\alpha \Delta t. \end{aligned}$$

Therefore the error term $\epsilon_{\Delta t}$ satisfies

$$\epsilon_{\Delta t} \leq C_7 \Delta t^2 + C_8 h + C_9 h^\alpha + C_{10} h^\alpha \Delta t.$$

For a grid point y, we can further derive

$$\begin{aligned} \left\| h_{2\Delta t}(y) - \widetilde{h}_{2\Delta t}(y) \right\| &\leq \left\| h_{\Delta t}(h_{\Delta t}(y)) - h_{\Delta t}(\widetilde{h}_{\Delta t}(y)) \right\| + \left\| h_{\Delta t}(\widetilde{h}_{\Delta t}(y)) - \widetilde{h}_{\Delta t}(\widetilde{h}_{\Delta t}(y)) \right\| \\ &\leq L_1 e^{L_2 \Delta t} \epsilon_{\Delta t} + \epsilon_{\Delta t} = L_3 \frac{e^{2L_2 \Delta t} - 1}{e^{L_2 \Delta t} - 1} \epsilon_{\Delta t}, \end{aligned}$$

and

$$\epsilon_{B\Delta t} = \left\| h_{B\Delta t}(y) - \widetilde{h}_{B\Delta t}(y) \right\| \leq L_3^B \frac{e^{L_2 B\Delta t} - 1}{e^{L_2 \Delta t} - 1} \epsilon_{\Delta t},$$

15

where
$$L_3 = \max(L_1, 1).$$

If y is not on grids, similarly we have

$$
\begin{aligned}
\epsilon_{B\Delta t} &\leq (N_1 + N_2)L_3^B \cdot \frac{e^{L_2 B\Delta t} - 1}{e^{L_2 \Delta t} - 1}\epsilon_{\Delta t} + \epsilon_{\Delta t} + C_{10}h^\alpha B\Delta t \\
&\leq (N_1 + N_2 + 1)L_3^B \cdot \frac{e^{L_2 B\Delta t} - 1}{e^{L_2 \Delta t} - 1}\epsilon_{\Delta t} + C_{10}h^\alpha B\Delta t \\
&= N \cdot \frac{e^{L_2 B\Delta t} - 1}{e^{L_2 \Delta t} - 1}\epsilon_{\Delta t} + C_{10}h^\alpha B\Delta t,
\end{aligned}
$$

and the recurrence relation is

$$
\begin{aligned}
\epsilon_{B^K \Delta t} &\leq N \cdot \frac{e^{L_2 B^K \Delta t} - 1}{e^{L_2 B^{K-1}\Delta t} - 1}\epsilon_{B^{K-1}\Delta t} + C_{10}h^\alpha B^K \Delta t \\
&\leq N^K \frac{e^{L_2 B^K \Delta t} - 1}{e^{L_2 \Delta t} - 1}\epsilon_{\Delta t} + C_{10}h^\alpha \sum_{k=0}^{K} N^k \frac{e^{L_2 B^K \Delta t} - 1}{e^{L_2 B^{K-k}\Delta t} - 1} B^{K-k}\Delta t \\
&\leq N^K \frac{e^{L_2 T} - 1}{L_2}\epsilon_{\Delta t} + C_{10}h^\alpha \frac{e^{LT} - 1}{L} \sum_{k=0}^{K} N^k.
\end{aligned}
$$

Hence we have
$$\epsilon_T \leq C(\Delta t^2 + h). \blacksquare$$

Remark 3.5 *Sometimes the coefficients of the linear h terms in the error estimate are much smaller than those of the higher order h terms, which makes the algorithm possess higher order convergence rate than linear, as observed in Example 2 of Section 4.1.*

4 Numerical examples and Applications

In this section we mainly study the examples appearing in classical mechanics where
$$H = \frac{1}{2}|\boldsymbol{\xi}|^2 + V(\boldsymbol{x}). \tag{37}$$

In the following examples, we compare the l^1 errors at time $t = T$ for h_t and f. The ratio of averaged number of special particles per iteration(NSP) over the number of total particles(NTP) are also presented in order to study the complexity of the algorithm. We use a second order symplectic solver $\Gamma_{\Delta t}$ presented in [6, 16]. For the interpolation operator $\mathcal{I}_1$, $\mathcal{I}_2$, we use the second order Lagrange polynomial interpolation [20].

4.1 Numerical examples

Example 1. Consider the 1D Liouville equation

$$f_t + \xi f_x - V_x f_\xi = 0,$$

on the computational domain

$$M = \left\{ (x,\xi) \in [0,1] \times [-0.8, 0.8] \;\middle|\; 0.02 \le H = V(x) + \frac{1}{2}\xi^2 \le 0.18 \right\}.$$

The potential $V(x)$ is given by

$$V(x) = \begin{cases} -0.4(x - 0.5)(x + 0.5), & 0 \le x < 0.5, \\ 0, & 0.5 \le x \le 1. \end{cases}$$

The initial data is
$$f(x,\xi,0) = 0,$$

and the boundary conditions are

$$
\begin{aligned}
f(1,\xi,t) &= \begin{cases} -25(\xi + 0.2)(\xi + 0.6)\sin(2\pi t) & -0.6 \le \xi \le -0.2, \\ 0 & \text{otherwise,} \end{cases} \\
f(0,\xi,t)|_{\xi>0} &= f(0,-\xi,t).
\end{aligned}
$$

This is a mixed boundary value problems, with inflow boundary condition at $x = 1$ and reflection boundary condition condition at $x = 0$.

The solution at time $T = 3$ is given in Figure 1. The exact solution is computed by solving the Hamiltonian system analytically. We present the l^1 error in Table 1, where the numerical solutions converges at about first order. In Table 2, the ratio of NSP over NTP with different mesh are shown. One could observe that the ratio is reduced linearly with the mesh size.

Table 1: the l^1 errors for different mesh sizes for Example 1

mesh	50×50	100×100	200×200	400×400
$h_T(x,\xi)$	2.46×10^{-3}	1.26×10^{-3}	6.33×10^{-4}	3.18×10^{-4}
$f(x,\xi,T)$	3.11×10^{-3}	1.69×10^{-3}	9.18×10^{-4}	4.79×10^{-4}

Example 2. Consider the 1D Liouville equation on the computational domain

$$M = \left\{ (x,\xi) \in [-1,1] \times [-0.8, 0.8] \;\middle|\; 0.02 \le H = V(x) + \frac{1}{2}\xi^2 \le 0.18 \right\},$$

Table 2: NSP versus NTP in Example 1

mesh	50×50	100×100	200×200	400×400
NSP	147	299	602	1212
NTP	1372	5364	21454	85826
ratio	10.71%	5.57%	2.81%	1.41%
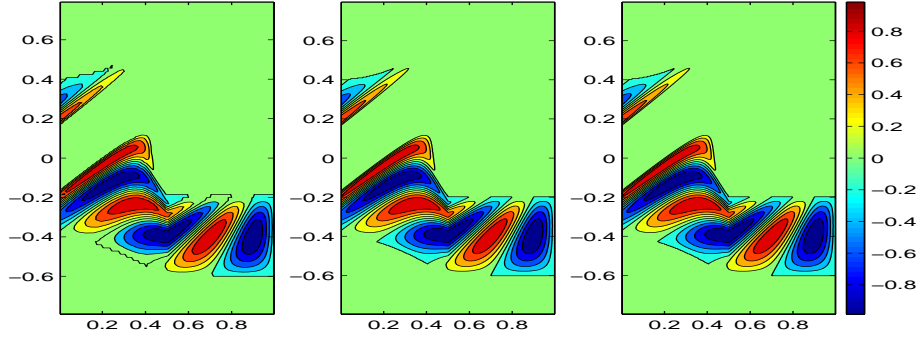
Figure 1: Example 1, phase space solution $f(x, \xi, t)$ at time $t = 3$. From left to right are the numerical solutions using 100×100 mesh, 400×400 mesh and the exact solution.

and the potential is given by (Figure 2)

$$V(x) = \begin{cases} 0.1(4x^2 - 1)^3, & -0.5 \leq x \leq 0.5, \\ 0, & \text{otherwise.} \end{cases}$$

The initial data is

$$f(x, \xi, 0) = 0, \tag{38}$$

and the boundary conditions are

$$f(1, \xi, t) = \begin{cases} -25(\xi + 0.2)(\xi + 0.6) \sin(2\pi t) & -0.6 \leq \xi \leq -0.2, \\ 0 & \text{otherwise,} \end{cases} \tag{39}$$

$$f(-1, \xi, t) = \begin{cases} -25(\xi - 0.2)(\xi - 0.6) \sin(2\pi t) & 0.2 \leq \xi \leq 0.6, \\ 0 & \text{otherwise.} \end{cases} \tag{40}$$

This is an inflow boundary condition problem. The solution at time $T = 2.5$ is given in Figure 3. The 'exact' solution is obtained by numerically solving the Hamiltonian system on a very fine mesh with a very small time step. We present the l^1 error and its convergence rate in Table 3. The numerical error is much small than in Example 1. The convergence rate is approaching

to the second order, which is better than the error estimate given in Section 3.2. This is explained in Remark 3.5. In Table 4, the ratios of NSP over NTP with different meshes are also shown.

Table 3: the l^1 errors for different mesh sizes for Example 2

mesh	50×50	100×100	200×200	400×400
$h_T(x, \xi)$	9.82×10^{-4}	3.01×10^{-4}	8.66×10^{-5}	2.39×10^{-5}
convergence rate	$- - -$	1.7060	1.7973	1.8574
$f(x, \xi, T)$	1.83×10^{-3}	5.53×10^{-4}	1.55×10^{-4}	4.23×10^{-5}
convergence rate	$- - -$	1.7265	1.8350	1.8667

Table 4: NSP versus NTP in Example 2

mesh	50×50	100×100	200×200	400×400
NSP	174	360	711	1440
NTP	1152	4532	18064	72292
ratio	15.10%	7.94%	3.94%	1.99%
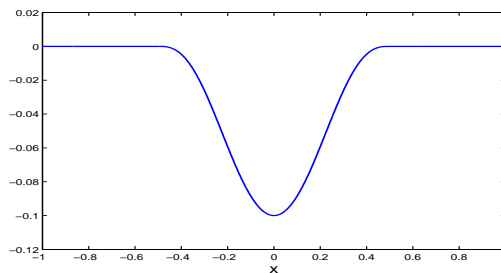
Figure 2: Example 2, potential $V(x)$.

4.2   Applications

In this subsection we study the applications in fast computation multivalued solutions to quasilinear PDEs. These problems arise in the semiclassical limit of the linear Schrödinger equation, in which the initial condition for (1) and (37) often takes the following form

$$f(\boldsymbol{x}, \boldsymbol{\xi}, 0) = \rho_0(\boldsymbol{x})\delta(\boldsymbol{\xi} - \boldsymbol{u}_0(\boldsymbol{x})), \tag{41}$$

19
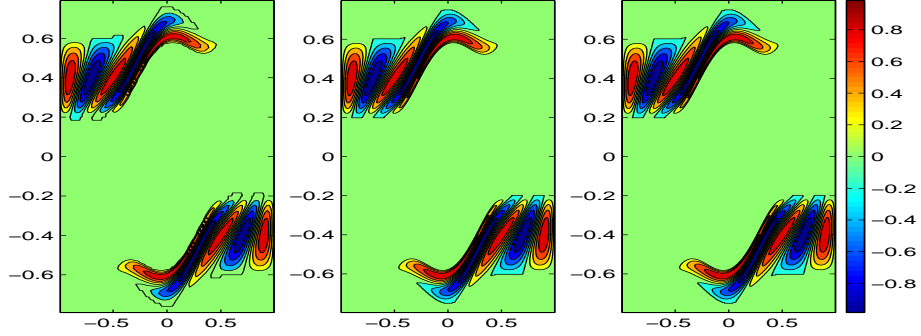
Figure 3: Example 2, phase space solution $f(x, \xi, t)$ at time $t = 2.5$. From left to right are the numerical solutions using 100×100 mesh, 400×400 mesh and the exact solution.

see for example [5, 17]. In most cases, we are interested in computing the multivalued physical observables, which can be constructed from the moments of f:

$$\rho(\boldsymbol{x}, t) = \int f(\boldsymbol{x}, \boldsymbol{\xi}, t) \mathrm{d}\boldsymbol{\xi},$$

$$\rho(\boldsymbol{x}, t)\boldsymbol{u}(\boldsymbol{x}, t) = \int \boldsymbol{\xi} f(\boldsymbol{x}, \boldsymbol{\xi}, t) \mathrm{d}\boldsymbol{\xi}.$$

The initial data (41) is singular, which potentially destroys the numerical accuracy. In [9], a decomposition technique was introduced to solve the multivalued physical observables for smooth potentials. This idea was extended for discontinuous potentials in [12]. See also [25, 26] for the discussions of the related delta function integrals. Below we will apply this new developed hybrid phase-flow method for fast computing the Liouville equation and constructing the multivalued physical observables.

Example 3. Consider the 1D Liouville equation on the computational domain

$$M = \left\{ (x, \xi) \in [-2, 2] \times [-1.6, 1.6] \,\middle|\, 0 \leq H = V(x) + \frac{1}{2}\xi^2 \leq 0.65 \right\},$$

with the discontinuous potential given by

$$V(x) = \begin{cases} 0.2, & x < 0, \\ 0, & x > 0. \end{cases}$$

The initial data is

$$f(x, \xi, 0) = \begin{cases} \delta(\xi - 0.9 + \frac{0.9}{4}(x + 2)^2), & -2 \leq x \leq 0, \\ \delta(\xi + 0.9 - \frac{0.9}{4}(x - 2)^2), & 0 < x \leq 2, \end{cases}$$

20

and the Dirichlet boundary conditions are

$$f(2, \xi, t) = \delta(\xi + 0.9),$$
$$f(-2, \xi, t) = \delta(\xi - 0.9).$$

This example was first proposed in [12], and the analytical velocity and density functions could be found in its Appendix. We output the numerical solutions of the density $\rho(x, t)$ and velocity $u(x, t)$ with different meshes against the exact solution at time $T = 1.8$ in Figure 4. In Table 5-6, we give the l^1 errors of the numerical solutions and the ratios of NSP over NTP. The convergence rate is nearly first order, which agrees with the discussion for interface problem in [13]. This is more accurate than the results in [12], where only halfth order was obtained [27].

Table 5: the l^1 errors for different mesh sizes for Example 3

mesh	100×100	200×200	400×400	800×800
$\rho(x,t)$	5.01×10^{-1}	2.90×10^{-1}	1.63×10^{-1}	7.77×10^{-2}
$u(x,t)$	4.82×10^{-2}	2.54×10^{-2}	1.44×10^{-2}	5.60×10^{-3}

Table 6: NSP versus NTP in Example 3

mesh	100×100	200×200	400×400	800×800
NSP	327	671	1394	2858
NTP	6600	26000	104800	417600
ratio	4.95%	2.58%	1.33%	0.68%

Example 4. Consider the 2D Liouville equation

$$f_t + \xi f_x + \eta f_y - V_x f_\xi - V_y f_\eta = 0,$$

on the computational domain

$$M = \left\{ (x, y, \xi, \eta) \in [-0.15, 0.21]^2 \times [0.2, 0.5]^2 \,\middle|\, 0.1 \leq V(x, y) + \frac{1}{2}(\xi^2 + \eta^2) \leq 0.26 \right\},$$

with the discontinuous potential given by

$$V(x, y) = \begin{cases} 0, & x + y > 0.11, \\ 0.1, & x + y < 0.11. \end{cases}$$
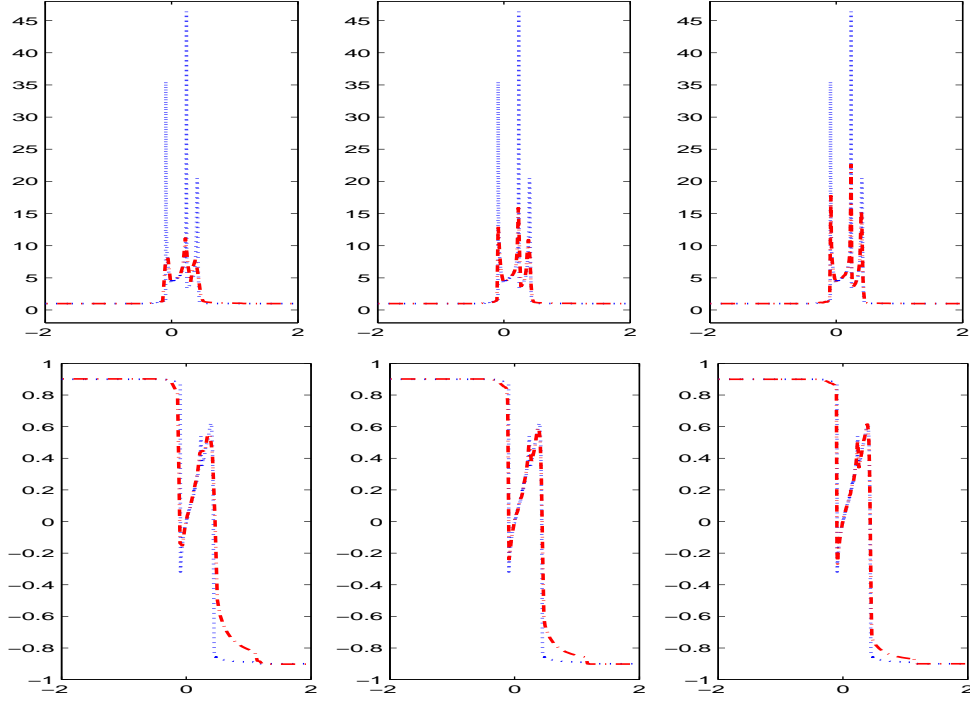
Figure 4: Example 3, density $\rho(x,t)$ (UP) and velocity $u(x,t)$ (DOWN) at time $t = 1.8$. The blue dotted lines are exact solutions and the red dashdot lines are numerical solutions. From left to right are the numerical solution using 100×100, 200×200 and 400×400 mesh.

The initial data is taken as

$$f(x,y,\xi,\eta,0) = \begin{cases} \delta(\xi - 0.2828)\delta(\eta - 0.2828), & -0.1 < x + y < 0.1, \ -0.1 < x - y < 0.1, \\ 0, & \text{otherwise.} \end{cases}$$

and the boundary conditions are

$$\begin{aligned} f(x,y,\xi,\eta,t)\big|_{(x,y)\in\partial M, \ (\xi,\eta)\cdot\vec{n}<0} &= 0, \\ \frac{\partial f}{\partial \vec{n}}(x,y,\xi,\eta,t)\big|_{(x,y)\in\partial M, \ (\xi,\eta)\cdot\vec{n}>0} &= 0. \end{aligned}$$

At time $T = 0.1886$, the exact density is

$$\rho(x,y,0.1886) = \begin{cases} \frac{2}{3}, & 0.11 < x + y < 0.255, \ -0.1 < x - y < 0.1, \\ 1, & 0.0067 < x + y < 0.11, \ -0.1 < x - y < 0.1, \\ 0, & \text{otherwise.} \end{cases}$$

We output the numerical solutions of the density $\rho(x,y,t)$ with different meshes against the exact density in Figure 5. In Table 7-8, we give the l^1 errors of the numerical solutions and the ratios of NSP over NTP, from which we can draw the same conclusion as in the end of the last example.

22

Table 7: the l^1 errors for different mesh sizes for Example 4

mesh	$26^2 \times 26^2$	$52^2 \times 52^2$	$104^2 \times 104^2$
$\rho(x,y,t)$	5.36×10^{-3}	2.49×10^{-3}	1.25×10^{-3}

Table 8: NSP versus NTP in Example 4

mesh	$26^2 \times 26^2$	$52^2 \times 52^2$	$104^2 \times 104^2$
NSP	53972	453690	3263199
NTP	226305	3680948	58532127
ratio	23.85%	12.33%	5.58%

5   Conclusion

In this paper, we propose a hybrid phase-flow method for solving the Liouville equation in the bounded domain where the flow map sits in the *variant* manifold of the *traditional* phase flow map. This hybrid phase flow method could help reduce the numerical difficulty when the *invariant* manifold of the phase flow given by the Liouville equation is big or unbounded. The stability and convergence of this algorithm is analyzed and several numerical examples and applications are presented to verify the accuracy and efficiency of this method.

Acknowledgement

References

[1] J. D. Benamou, *Direct computation of multivalued phase space solutions for Hamilton-Jacobi equations*, Comm. Pure Appl. Math. **52** (1999), pp. 1443-1457.

[2] L.T. Cheng, H.L. Liu and S. Osher, *Computational high-frequency wave propagation using the level set method, with applications to the semiclassical limit of Schrödinger equations*, Communications in Mathematical Sciences **1** (2003), pp. 593-621.

[3] B. Engquist and O. Runborg, *Computational high frequency wave propagation*, Acta Numerica **12** (2003), pp. 181-266.
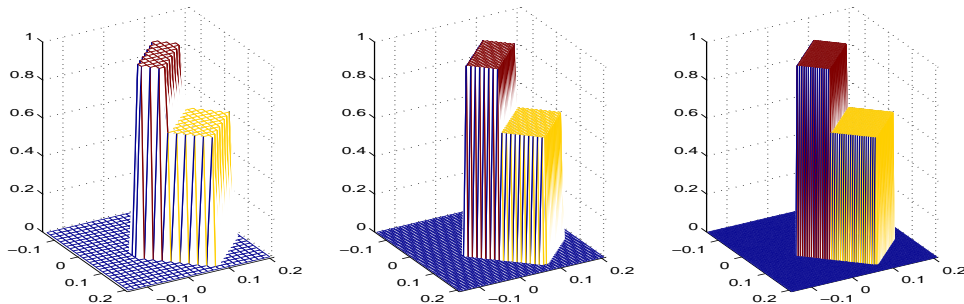
Figure 5: Example 4, density $\rho(x, y, t)$ at time $t = 0.1886$. ¿From left to right are the numerical solutions using $26^2 \times 26^2$ mesh, $52^2 \times 52^2$ mesh and the exact solution.

[4] B. Engquist, O. Runborg and A. K. Tornberg, *High frequency wave propagation by the segment projection method*, J. Comp. Phys. **178** (2002), pp. 373-390.

[5] P. Gérard, P.A. Markowich, N.J. Mauser and F. Poupaud, *Homogenization limits and Wigner transforms*, Communications on Pure and Applied Mathematics **50** (1997), pp. 321-377.

[6] E. Hairer, C. Lubich and G. Wanner, *Geometric Numerical Integration: Structure-preserving Algorithms for Ordinary Differential Equations*, Springer-Verlag, Berlin, 2002.

[7] S. Jin, *Recent computational methods for high frequency waves in heterogeneous media*, preprint.

[8] S. Jin and X.T. Li, *Multi-phase computations of the semiclassical limit of the Schrödinger equation and related problems: Whitham vs. Wigner*, Physica D **182** (2003), pp. 46-85.

[9] S. Jin, H.L. Liu, S. Osher and R. Tsai, *Computing multivalued physical observables for the semiclassical limit of the Schrödinger equation*, Journal of Computational Physics **205** (2005), pp. 222-241.

[10] S. Jin and K. Novak, *A Semiclassical Transport Model for Two-dimensional Thin Quantum Barriers*, Journal of Computational Physics **226** (2007), pp. 1623-1644.

[11] S. Jin and S. Osher, *A level set method for the computation of multivalued solutions to quasi-linear hyperbolic PDEs and Hamilton-Jacobi Equations*, Communications in Mathematical Sciences **1** (2003), pp. 575-591.

[12] S. Jin and X. Wen, *Hamiltonian-preserving schemes for the Liouville equation of discontinuous potential*, Communications in Mathematical Sciences **3** (2005), pp. 285-315.

[13] S. Jin, H. Wu and Z.Y. Huang, *A Hybrid Phase-Flow Method for Hamiltonian Systems with Discontinuous Hamiltonians*, SIAM J. Sci. Comp. **31** (2008), pp. 1303-1321.

[14] S. Jin, H. Wu and X. Yang, *Gaussian beam methods for the Schrodinger equation in the semi-classical regime: Lagrangian and Eulerian formulations*, Commun. Math. Sci. **6** (2008), no. 4, pp. 995-1020.

[15] J.B. Keller and R.M. Lewis, *Asymptotic methods for partial differential equations: the reduced wave equation and Maxwell's equations*, Surveys in applied mathematics **1** (1995), pp. 1-82.

[16] B. Leimkuhler and S. Reich, *Simulating Hamiltonian Dynamics*, Cambridge University Press, 2004.

[17] P.L. Lions and T. Paul, *Sur les measures de Wigner*, Revista Matemática Iberoamericana **9** (1993), pp. 553-618.

[18] G. Papanicolaou and L. Ryzhik, *Waves and Transport*, IAS/Park City Math. Series **5**, 305-382, 1998, L. Carrarelli and Weinan E eds.

[19] M. M. Popov, *A new method of computation of wave fields using gaussian beams*, Wave Motion **4** (1982), pp. 85-97.

[20] K. Rainer, *Numerical Analysis*, Springer, New York, 1998.

[21] J. Ralston, *Gaussian beams and the propagation of singularities*, Studies in PDEs, MAA stud. Math. **23** (1982), pp. 206-248.

[22] O. Runborg, *Mathematical models and numerical methods for high frequency waves*, Commun. Comput. Phys. **2** (2007), no. 5, pp. 827–880.

[23] C. Sparber, P.A. Markowich and N.J. Mauser, *Wigner functions versus WKB-methods in multivalued geometrical optics*, Asymptotic Analysis **33** (2003), pp. 153-187.

[24] N. M. Tanushev, *Superpositions and higher order Gaussian beams*, Commun. Math. Sci. **6** (2008), no. 2, pp. 449-475.

[25] X. Wen, *High order numerical methods to a type of delta function integrals*, Journal of Computational Physics **226** (2007), pp. 1952-1967.

[26] X. Wen, *High order numerical quadratures to one dimensional delta function integrals*, preprint.

[27] X. Wen and S. Jin, *The l^1-error estimates for a Hamiltonian-preserving scheme to the Liouville equation with piecewise constant coefficients*, preprint.

[28] L.X. Ying and E.J. Candés, *The Phase flow method*, Journal of Computational Physics **220** (2006), pp. 184-215.